

Article

# Formation of High-Purity Indium Oxide Nanoparticles and Their Application to Sensitive Detection of Ammonia

Sanjeev K. Bhardwaj<sup>1,2</sup>, Neha Bhardwaj<sup>1,2</sup>, Manil Kukkar<sup>1,2</sup>, Amit L. Sharma<sup>1,2</sup>,  
Ki-Hyun Kim<sup>3,\*</sup> and Akash Deep<sup>1,2,\*</sup>

Received: 22 October 2015; Accepted: 11 December 2015; Published: 17 December 2015  
Academic Editor: W. Rudolf Seitz

<sup>1</sup> Central Scientific Instruments Organisation (CSIR-CSIO), Sector 30 C, Chandigarh 160030, India; sanjeevbhardwaj1988@gmail.com (S.K.B.); nehavashisht1989@gmail.com (N.B.); er.manilkukkar@gmail.com (M.K.); amitsharma\_csio@yahoo.co.in (A.L.S.)

<sup>2</sup> Academy of Scientific and Innovative Research, CSIR-CSIO, Sector 30 C, Chandigarh 160030, India

<sup>3</sup> Department of Civil & Environmental Engineering, Hanyang University, 222 Wangsimni-Ro, Seoul 04763, Korea

\* Correspondences: kkim61@hanyang.ac.kr (K.-H.K.); dr.akashdeep@gmail.com (A.D.);  
Tel.: +82-2-2220-2325 (K.-H.K.); +91-172-265-7811 (ext. 452) (A.D.);  
Fax: +82-2-2220-1945 (K.-H.K.); +91-172-265-7287 (A.D.)

**Abstract:** High-purity In<sub>2</sub>O<sub>3</sub> nanoparticles were recovered from scrap indium tin oxide substrates in a stepwise process involving acidic leaching, liquid-liquid extraction with a phosphine oxide extractant, and combustion of the organic phase. The morphological and structural parameters of the recovered nanoparticles were investigated to support the formation of the desired products. These In<sub>2</sub>O<sub>3</sub> nanoparticles were used for sensitive sensing of ammonia gas using a four-probe electrode device. The proposed sensor offered very quick response time (around 10 s) and highly sensitive detection of ammonia (at a detection limit of 1 ppm).

**Keywords:** indium oxide nanoparticles; recovery; scrap; sensing; ammonia

## 1. Introduction

Indium oxide (In<sub>2</sub>O<sub>3</sub>) nanostructures have a direct bandgap of 3.55–3.75 eV with versatile applicability to selective sensors, solar cells, flat-panel displays, and photocatalytic devices [1–4]. The wide band gap of In<sub>2</sub>O<sub>3</sub> suggests their potential applicability under room temperature conditions, like other wide band gap semiconductors, e.g., GaN, ZnO, TiO<sub>2</sub>, and diamond. A number of synthesis methods have been proposed to grow In<sub>2</sub>O<sub>3</sub> nanostructures in different forms such as nanowires, nanowire arrays, nanocubes, octahedrons, hollow microspheres, and nanorod bundles (and spheres) [5]. For the synthesis of indium oxide nanostructures, the following techniques have commonly been employed: electrodeposition, chemical bath deposition, chemical vapour deposition, molecular beam epitaxy, hydrothermal, and sol-gel synthesis [6]. Chemical deposition is a simple and low cost method. However, wet chemical synthesis often requires a variety of controlling agents to adjust the shape of nanocrystals. The use of such additives (e.g., complexing agents, surfactants, and pH regulating agents) makes the synthesis methods complicated and costly. Sometimes those additives can also remain as impurities in the final product. Electrodeposition and oxidizing methods are used preferably to obtain indium oxide spheres [7]. The use of chemical vapor deposition and annealing of In(OH)<sub>3</sub> precursor have been proposed as possible routes for the synthesis of In<sub>2</sub>O<sub>3</sub> nanoparticles [8,9]. Hard and soft template-based synthesis of different In<sub>2</sub>O<sub>3</sub> micro- and nanostructures has also been proposed by several researchers [10–13]. Use of polystyrene beads, polymethylmethacrylate, and carbon materials

has been reported in hard template-based synthesis, whereas vesicles, microemulsion droplets, and micelles have been used in soft template-based synthesis. In the preparation of  $\text{In}_2\text{O}_3$  particles, application of the former was preferred over the latter due to superiority in terms of size, shape, shell thickness, and surface morphology.

The application of  $\text{In}_2\text{O}_3$  nanoparticles for sensing ammonia has been demonstrated by many researchers [14–16]. However, most of those reported sensors were designed to operate at elevated temperatures. In some cases, response times of 30 s or more have been reported [14,15]. Other studies have also addressed the possibility of sensing ammonia under room temperature conditions without providing detailed information [15].  $\text{Ti}^{4+}$  ion doped  $\text{In}_2\text{O}_3$  has also been proposed for such an application with the detection of  $\text{NH}_3$  in the 5–1000 ppm range [16].

Because indium is a rare element, its regeneration from scrap materials is important. Leaching has been proposed as an effective method to recover metallic components from scrap materials; however, it is difficult to obtain pure products using such an approach [17,18]. Liquid-liquid extraction is a popular hydrometallurgical technique that allows pre-concentration and purification of metals from leaching solutions [19–21]. In this research, we propose a new facile synthesis route for the formation of  $\text{In}_2\text{O}_3$  nanoparticles from scrap indium tin oxide substrates based on an extraction-calcination route. The template-free method is capable of producing homogeneously porous  $\text{In}_2\text{O}_3$  nanoparticles. Compared to the above listed techniques, the process proposed herein is suitable for the enhanced recovery of the desired product from waste materials; it was proven to provide the *in-situ* separation of pure indium from other impurities (liquid-liquid extraction step). The utility of these  $\text{In}_2\text{O}_3$  nanoparticles was demonstrated for sensitive sensing of ammonia gas by a four-probe sensor device. The synthesized  $\text{In}_2\text{O}_3$  nanoparticles allowed sensitive (1 ppm) detection of ammonia.

## 2. Experimental

### 2.1. Materials

To build biosensing platform proposed in this research, scrap indium tin oxide (ITO) collected through the various optimization procedures tested in this study were used as the source of indium. The metal extractant “Cyanex 923” is a mixture of four alkyl phosphine oxides ( $\text{R}_3\text{P} = \text{O}$ ,  $\text{R}'\text{R}_2\text{P} = \text{O}$ ,  $\text{R}_2\text{R}'\text{P} = \text{O}$ , and  $\text{R}_3'\text{P} = \text{O}$ , where R and R' represent *n*-octyl and *n*-hexyl hydrocarbon chains, respectively) marketed by the Cytec Canada Inc. (Paterson, NJ, USA) All other reagents and solvents used in this work were high-purity products from Sigma Aldrich/Merck (New Delhi, India).

### 2.2. Method

About 2 g of the scrap ITO substrates were cut in small pieces and then treated with 10 mL of 50% *aqua regia* solution (a 1:3 (V/V) mixture of  $\text{HNO}_3$  and  $\text{HCl}$ ) for 1 h at 90 °C. The leaching solution (L1) was collected after this reaction. The conductivity of the remaining substrates was measured in order to verify the removal of the ITO layer. None the tested substrates showed any conductivity, indicating that the ITO layer was removed from the glass surface.

The leaching solution “L1” was diluted with deionized water to a volume four-times the original. The concentrations of the metals (indium, tin) in the solution were determined by inductively coupled plasma-mass spectrometry (ICP-MS, ELAN DRC-e, Perkin Elmer, Boston, MA, USA). The extraction of indium was then carried out in 0.05 mol/L toluene (Cyanex 923) solution. For this, 40 mL of the diluted “L1” solution was equilibrated with 10 mL of Cyanex 923 solution for 5 min at room temperature. The aqueous and organic layers were allowed to settle, and the organic phase (O1) was decanted. ICP-MS analysis of the aqueous phase was then carried out to determine the content of extracted metal.

For the preparation of  $\text{In}_2\text{O}_3$  nanoparticles, the solution “O1” was transferred into a platinum crucible and then combusted in a furnace at 500 °C for 2 h. The solvent was evaporated to produce finely assembled  $\text{In}_2\text{O}_3$  particles, which were characterized by field-emission scanning electron microscopy-energy dispersive X-ray spectroscopy (FE-SEM-EDX, 4300/SN Hitachi, Tokyo, Japan),

transmission electron microscopy (TEM, JEOL, Tokyo, Japan), Fourier transform infrared spectroscopy (FTIR, iS10, Nicolet, Madison, WI, USA), and X-ray diffraction spectroscopy (D8 Advance, Bruker, Mumbai, India). Surface area was measured using an Autosorb 1C BET Surface Area & Pore Volume Analyzer Quantachrome (Jacksonville, FL, USA). The particle size distribution analysis was carried out with a Zetasizer Nano ZS from Malvern (Worcestershire, UK).

The ammonia sensing device was fabricated by drop-casting the  $\text{In}_2\text{O}_3$  suspension onto a four-probe gold electrode. The above suspension was prepared by treating 50 mg of the prepared  $\text{In}_2\text{O}_3$  nanoparticulates with a 20 mL mixture of ethanol and chloroform (1:1). The mixture was sonicated for 30 min and then left for 12 h. Large particles were separated by centrifugation at 1000 rpm. This treatment was repeated for three times to obtain a well dispersed transparent colloidal solution for drop casting the nanoparticle layer.

The  $\text{In}_2\text{O}_3$  drop-cased electrode was allowed to dry and then tested for detection of ammonia. The schematic set-up of the gas sensing chamber is shown in Figure 1. Suitably diluted ammonia solutions were introduced in the sensing chamber, and the gas was dispersed by heating so as to obtain effective gas concentrations in the range of 0.1–100 ppm. These concentrations were determined by first preparing ammonia solutions of known molarity and considering their maximum diffusion inside the gas chamber with a volume of 5.7 L. The sensitivity “S” of the sensor was estimated according to the following equation:

$$S = R_a/R_g$$

where  $R_a$  is the resistance of the sensor in air and  $R_g$  is the resistance after introducing ammonia into the test chamber. The response of the sensor was investigated using a constant current source and an electrometer (Keithley, Bangalore, India).

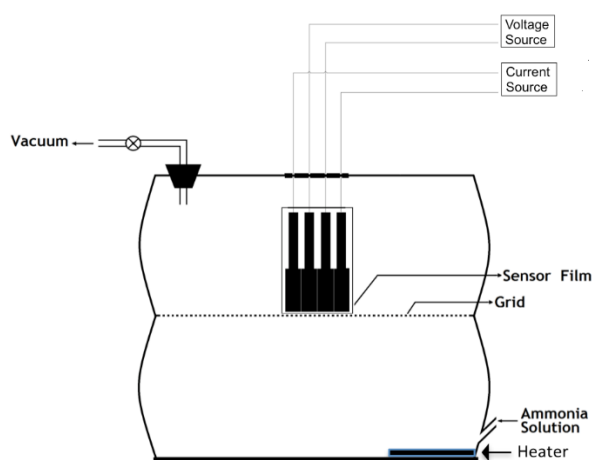


Figure 1. Schematic of the ammonia sensing setup.

### 3. Results and Discussion

#### 3.1. Solution Compositions

The ICP-MS analysis of solution “L1” before extraction with Cyanex 923 showed the following: 15 mg/L of indium and 2 mg/L of tin. The literature reports that acidic leaching of ITO is useful to solubilize indium, while the leaching of tin remains is only about 10% [21]. Because the target substrates were scraps collected during optimization studies for the development of biosensors, the presence of some components like carbon, nitrogen, and sulfur in the leaching solution is expected. For complete analysis, a fraction of the “L1” solution was completely evaporated on a silicon wafer and analyzed using an FE-SEM/EDX, as shown in Figure 2. The presence of all the expected components (*i.e.*, indium, tin, carbon, nitrogen, and sulfur) is confirmed in this microstructure. The results of

ICP-MS analysis after extraction with Cyanex 923 were as follows: indium, 0.1 mg/L and tin, 2 mg/L. This suggests that indium was almost completely transferred to the organic phase with negligible extraction of tin. This particular study clearly highlights the selective extraction of indium by Cyanex 923 solution. The extraction of metal ions with Cyanex 923 takes place via a solvation process that depends upon the acidity in the aqueous phase. The quantitative extraction of In(III) from dilute to moderate HCl solutions can be attributed to the formation of extractable  $\text{InCl}_3$  species. As tin forms neutral or cationic chloro-species only in concentrated HCl conditions, its extraction was negligible under the present aqueous phase conditions.

The results of these studies confirm the effectiveness of the proposed leaching-extraction technique for obtaining pure indium solution from scrap ITO targets. The suggested method can also be applied to other types of waste materials. The proposed process involves the solvent extraction separation of indium from a leaching solution. Hence, a similar strategy can also be applied to other waste materials.

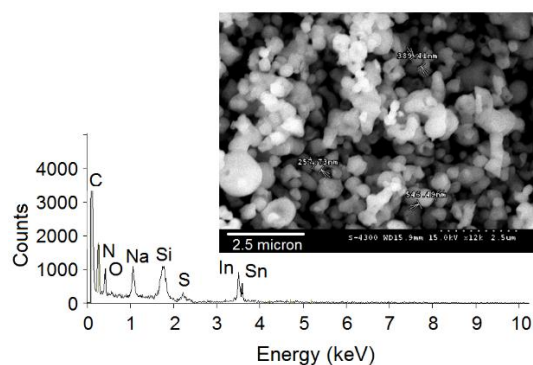
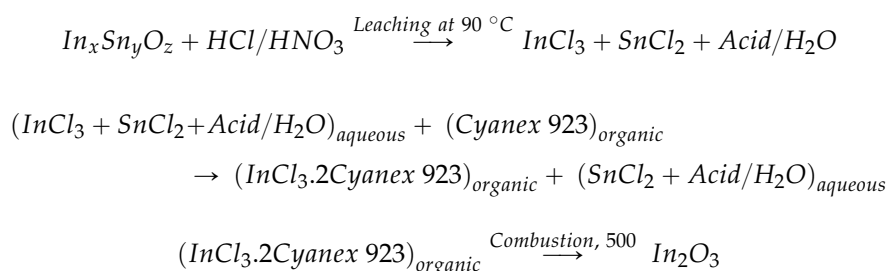


**Figure 2.** FE-SEM and EDX analysis of the solution obtained after the leaching step on scrap ITO substrates.

### 3.2. Characterization of $\text{In}_2\text{O}_3$ Nanoparticles

The leaching, extraction, and combustion processes can be explained by the following chemical equations:



In the given composition of the leaching reagent, it can be assumed that indium should primarily be dissolved as  $\text{InCl}_3$ . The extraction of indium chloro-complex by Cyanex 923 has been described in the literature through a solvation mechanism [22]. As discussed in the previous section, the extraction of indium from the leaching solution “L1” was selective towards tin. Combustion of the indium-Cyanex 923 complex led to the formation of porous nanoparticles of  $\text{In}_2\text{O}_3$ , as evidenced by FE-SEM and TEM investigations (Figures 3 and 4a, respectively). The obtained product and its EDX analysis confirm the formation of pure homogeneous nanoparticles of  $\text{In}_2\text{O}_3$  free from other impurities. The particle size distribution analysis of the  $\text{In}_2\text{O}_3$  dispersion is shown in Figure 4b. A polydispersity index of 0.24 suggests that the  $\text{In}_2\text{O}_3$  dispersant should contain homogenous particles. The average particle diameter was estimated as 100 nm.

The morphology of these particles indicates the porous nature of the nanoparticles. The estimated Langmuir surface area of the  $\text{In}_2\text{O}_3$  nanoparticles averaged as  $211 \text{ m}^2 \text{ g}^{-1}$ . The purity of the synthesized

product has also been cross-checked with ICP-MS analysis. A digested sample of  $\text{In}_2\text{O}_3$  was found to be free from other elements, namely, Sn, Fe, Al, Cr, Na, Cu, and Cr.

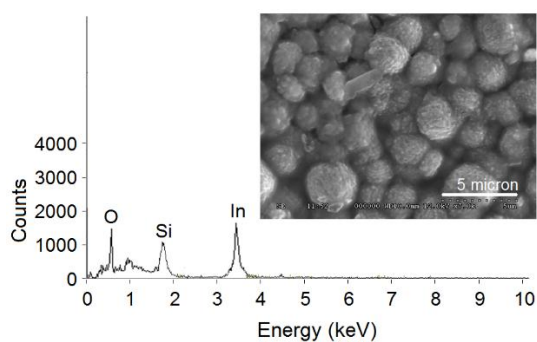


**Figure 3.** FE-SEM and EDX analyses of the synthesized  $\text{In}_2\text{O}_3$  nanoparticles.

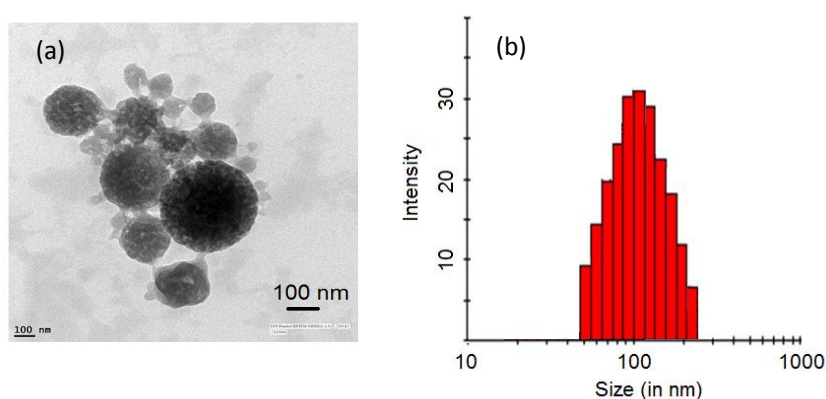


**Figure 4.** (a) TEM analysis and (b) Particle size distribution (DLS) of the synthesized  $\text{In}_2\text{O}_3$  nanoparticles.

XRD analysis of the sample is shown in Figure 5. The presence of strong and sharp diffraction peaks confirms synthesized product as a crystalline material.

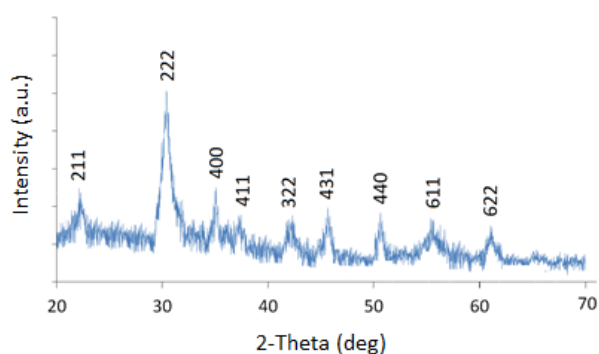


**Figure 5.** XRD analysis of the synthesized  $\text{In}_2\text{O}_3$  nanoparticles.

All the diffraction peaks can be indexed to body centered cubic (bcc) structured  $\text{In}_2\text{O}_3$ . The XRD data are in agreement with the standard data from JCPDS card No. 65-3170 as well as results of previous studies [14,23,24]. There were no impurities phases present. Figure 6 shows the FTIR spectra of the recovered  $\text{In}_2\text{O}_3$  nanoparticles. The thermal treatment of the complex produced pure  $\text{In}_2\text{O}_3$  nanoparticles. The bands around  $1630$  and  $1050\text{ cm}^{-1}$  are attributed to the absorption of hydroxyls and absorption of C-O vibration, respectively. Broad absorptions around  $600\text{ cm}^{-1}$  are attributed to

the metal oxide vibrations. The results of the FTIR analysis were comparable to those of the earlier reports, e.g., [25].

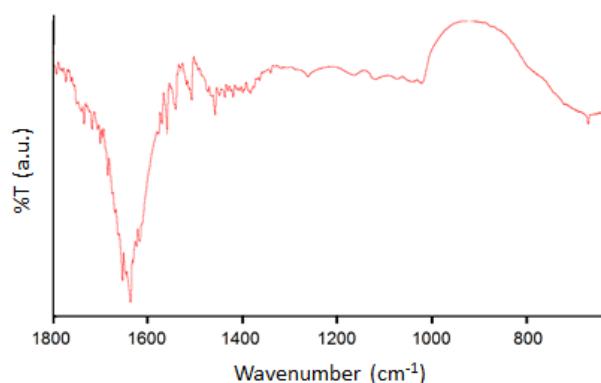


Figure 6. FTIR analysis of the synthesized  $\text{In}_2\text{O}_3$  nanoparticles.

### 3.3. Use of $\text{In}_2\text{O}_3$ Nanoparticles for Ammonia Sensing

The results obtained from the application of recovered  $\text{In}_2\text{O}_3$  nanoparticles for the sensing of ammonia are shown in Figures 7 and 8.

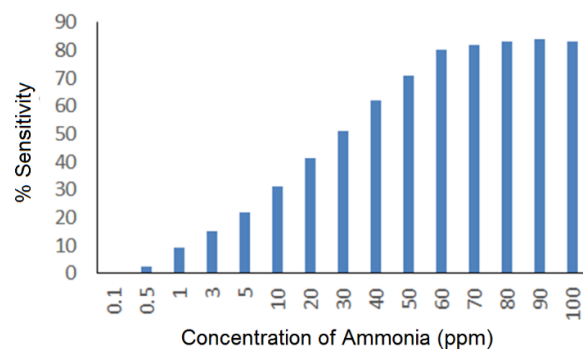


Figure 7. Sensitivity of the  $\text{In}_2\text{O}_3$  nanoparticle sensor at different concentrations of ammonia.

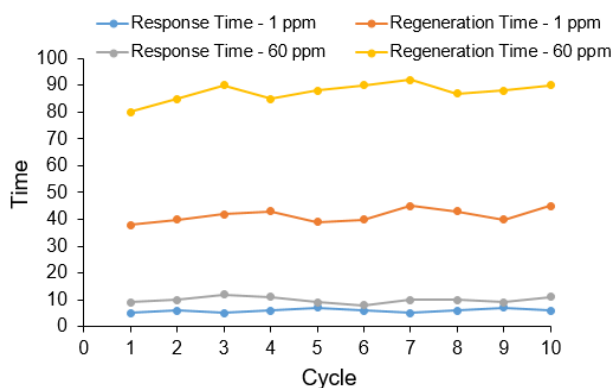


Figure 8. Response and recovery of the  $\text{In}_2\text{O}_3$  nanoparticle sensor at low (A: 1 ppm) and high concentrations of ammonia (B: 60 ppm) during successive cycles.

As shown, the sensor can very sensitively detect the presence of  $\text{NH}_3$  molecules in a linear detection range of 1 to 60 ppm. Exposure of the sensor to higher concentrations led to saturation. The investigations on the response time showed fast response of less than 10 s for 1 ppm, while it is slightly

extended above 10 s for 60 ppm. The recovery times (Figure 8) measured at two different concentrations (1 and 60 ppm) were around 50 and 100 s, respectively. Ammonia behaved as a reducing gas for the  $\text{In}_2\text{O}_3$  sensor. It is known that  $\text{In}_2\text{O}_3$  in a slightly non-stoichiometric form contains a large number of localized centers with trapped electrons, which explains the observed sensitivity in the sensor's response at room temperature. This response behavior indicates the possibility of many surface sites suitable for reaction with ammonia. A large proportion of the sensitivity resistance of the sensor is due to surface reactions. Upon exposure to air, oxygen species are adsorbed on the surface of a metal oxide semiconductor gas sensor. These oxygen species then undergo ionization by electrons from the material's conduction band to form such species as  $\text{O}^{2-}$ . The resistance of  $\text{In}_2\text{O}_3$  semiconducting material is expected to increase in the presence of air due to relatively low concentration of free electrons in the conduction band. The presence of reducing gas ( $\text{NH}_3$ ) initiates the surface reaction between the oxygen species and analyte gas, causing the release of electrons trapped in the ionized oxygen species back into the conduction band, which ultimately lowers the resistance. This result is typical behavior for indium oxide as an n-type semiconductor. The porous structure of  $\text{In}_2\text{O}_3$  is an important reason for the sensitivity of the sensor. Porosity of the surfaces helps in absorbing more oxygen to generate more ionized oxygen species. The increased surface-to-volume ratio of the porous nanostructure should increase the absorption and ionization of oxygen. The sensing performance of  $\text{In}_2\text{O}_3$  obtained at two different calcination temperatures (*i.e.*, 500 and 700 °C) is summarized in Table 1. It indicated that the performance of the above two sets of the particles was not much different from each other.

**Table 1.** Relative performance of  $\text{In}_2\text{O}_3$  for sensing ammonia at two different calcination temperatures between 500 and 700 °C.

Concentration of $\text{NH}_3$	Parameters Observed for Material Calcined at 500 °C			Parameters Observed for Material Calcined at 700 °C		
	Sensitivity	Response Time	Recovery Time	Sensitivity	Response Time	Recovery Time
5 ppm	22 ± 2%	10 ± 4	50 ± 10	25 ± 2%	8 ± 4	40 ± 6
60 ppm	78 ± 3%	10 ± 4	100 ± 10	85 ± 4%	10 ± 4	85 ± 10

The chemiresistive sensors are potent enough to develop fast, inexpensive, and portable devices for sensing various gases. However, their sensitivity toward humidity is often found as a limiting factor in acquiring the reliable and reproducible results. To resolve this problem, the sensor can be designed with a reference line for blank controls as desired. As checked in the lab, the sensitivity of the sensor proposed herein toward 5 ppm ammonia/50% relative humidity was around 50:1. It might be pertinent to discuss here that various sensor designs have been proposed in the literature to counter this humidity-related problem. The interfering effect of humidity was tackled by virtue of the difference in thermal conductivity between air and water vapor. Application of standard passivation layer of the CMOS chip as the humidity sensing element, subtraction circuit, and self-calibrated humidity sensor may also be used to develop a complete sensing system [26]. As another approach to compensate humidity, a separate in-chamber humidity sensor was employed [27]. The data were successfully processed for post feature extraction compensation of humidity to accurately adjust bias in the measured humidity.

The attainment of required selectivity is another issue for the gas sensing devices. One of the approaches to handle this situation is to add computational hardware/software for the pattern recognition analysis of various output sensing signals [28]. Recently, some researchers have proposed the design of sensors that can supply an assortment of independent features each of which responds to the various analyte gases. The collective output of these features could be treated via simple pattern recognition methods against the complicated mixtures [29]. The selective detection of gases and volatile organic compounds can also be achieved by considering multiple independent parameters of

a sensor, e.g., voltage threshold, hole mobility, subthreshold swing, *etc.* as input for artificial neural network which, in turn, can be trained in its ensemble to make the targeted detection.

#### 4. Conclusions

For the first time, the recycling of used indium tin oxide substrate into conducting indium oxide nanoparticles is described. Pure (>98%) indium solution was retrieved from the leaching solution of scrap ITO targets using Cyanex 923 extractant. This solution was then subjected to combustion in order to produce nanoparticles. The synthesized  $\text{In}_2\text{O}_3$  nanoparticles, when tested by various instrumental methodologies, were shown to be highly pure and useful for detection of ammonia gas. The proposed strategy can also be extended to other waste materials containing indium for its efficient recycling. As demonstrated in this study, the recovered product can be used as a gas sensing material in addition to other potential applications.

**Acknowledgments:** The authors are thankful to the Director of CSIR-CSIO, Chandigarh, India, for providing infrastructure facilities. The research was funded by CSIR, India grant No. OMEGA/PSC0202. The corresponding author (Ki-Hyun Kim) also acknowledges partial support by a grant from the National Research Foundation of Korea (NRF) funded by the Ministry of Education, Science and Technology (MEST) (No. 2009-0093848).

**Author Contributions:** Sanjeev K. Bhardwaj and Neha Bhardwaj carried out the leaching and solvent extraction experiments, while Manil Kukkar optimized the nanoparticle formation through combustion. Amit L. Sharma investigated the structural parameters and material purity. Ki-Hyun Kim compiled and organized the manuscript and data evaluation. Akash Deep conceptualized and supervised the experimental work.

**Conflicts of Interest:** The authors declare no conflict of interest.

#### References

- George, P.P.; Gedanken, A. Synthesis, Characterization, and Photoluminescence Properties of  $\text{In}_2\text{O}_3$  Nanocrystals Encapsulated by Carbon Vesicles and Neat  $\text{In}_2\text{O}_3$  Nanocrystals Generated by the RAPET Technique. *Eur. J. Inorg. Chem.* **2008**, *2008*, 919–924. [[CrossRef](#)]
- Zhang, D.; Liu, Z.; Li, C.; Tang, T.; Liu, X.; Han, S.; Lei, B.; Zhou, C. Detection of  $\text{NO}_2$  down to ppb Levels Using Individual and Multiple  $\text{In}_2\text{O}_3$  Nanowire Devices. *Nano Lett.* **2004**, *4*, 1919–1924. [[CrossRef](#)]
- Cui, J.; Wang, A.; Edleman, N.L.; Ni, J.; Lee, P.; Armstrong, N.R.; Marks, T.J. Indium Tin Oxide Alternatives—High Work Function Transparent Conducting Oxides as Anodes for Organic Light-Emitting Diodes. *Adv. Mater.* **2001**, *13*, 1476–1480. [[CrossRef](#)]
- Zhao, P.; Huang, T.; Huang, K. Fabrication of Indium Sulfide Hollow Spheres and Their Conversion to Indium Oxide Hollow Spheres Consisting of Multipore Nanoflakes. *J. Phys. Chem. C* **2007**, *111*, 12890–12897. [[CrossRef](#)]
- Liu, Z.; Zhang, D.; Han, S.; Li, C.; Tang, T.; Jin, W.; Liu, X.; Lei, B.; Zhou, C. Laser Ablation Synthesis and Electron Transport Studies of Tin Oxide Nanowires. *Adv. Mater.* **2003**, *15*, 1754–1757. [[CrossRef](#)]
- Shinde, D.V.; Ahn, D.Y.; Jadhav, V.V.; Lee, D.Y.; Shrestha, N.K.; Lee, J.K.; Lee, H.W.; Maneb, R.S.; Han, S.-H. A coordination chemistry approach for shape controlled synthesis of indium oxide nanostructures and their photoelectrochemical properties. *J. Mater. Chem. A* **2014**, *2*, 5490–5498. [[CrossRef](#)]
- Zheng, M.; Zhang, L.; Zhang, X.; Zhang, J.; Li, G. Fabrication and optical absorption of ordered indium oxide nanowire arrays embedded in anodic alumina membranes. *Chem. Phys. Lett.* **2001**, *334*, 298–302. [[CrossRef](#)]
- Dai, Z.R.; Pan, Z.W.; Wang, Z.L. Novel Nanostructures of Functional Oxides Synthesized by Thermal Evaporation. *Adv. Funct. Mater.* **2003**, *13*, 9–24. [[CrossRef](#)]
- Li, B.; Xie, Y.; Jing, M.; Rong, G.; Tang, Y.; Zhang, G.  $\text{In}_2\text{O}_3$  Hollow Microspheres: Synthesis from Designed  $\text{In}(\text{OH})_3$  Precursors and Applications in Gas Sensors and Photocatalysis. *Langmuir* **2006**, *22*, 9380–9385. [[CrossRef](#)] [[PubMed](#)]
- Tseng, W.J.; Tseng, T.-T.; Wu, H.-M.; Her, Y.-C.; Yang, T.-J. Facile Synthesis of Monodispersed  $\text{In}_2\text{O}_3$  Hollow Spheres and Application in Photocatalysis and Gas Sensing. *J. Am. Ceram. Soc.* **2013**, *96*, 719–725. [[CrossRef](#)]
- Kim, S.-J.; Hwang, I.-S.; Choi, J.-K.; Kang, Y.C.; Lee, J.-H. Enhanced  $\text{C}_2\text{H}_5\text{OH}$  sensing characteristics of nano-porous  $\text{In}_2\text{O}_3$  hollow spheres prepared by sucrose-mediated hydrothermal reaction. *Sens. Actuators B Chem.* **2011**, *155*, 512–518. [[CrossRef](#)]

12. Hyodo, T.; Inoue, H.; Motomura, H.; Matsuo, K.; Hashishin, T.; Tamaki, J.; Shimizu, Y.; Egashira, M. NO<sub>2</sub> sensing properties of macroporous In<sub>2</sub>O<sub>3</sub>-based powders fabricated by utilizing ultrasonic spray pyrolysis employing polymethylmethacrylate microspheres as a template. *Sens. Actuators B Chem.* **2010**, *151*, 265–273. [[CrossRef](#)]
13. Zhao, H.; Dong, H.; Zhang, L.; Wang, X.; Yang, H. Controlled synthesis and photocatalytic properties of porous hollow In<sub>2</sub>O<sub>3</sub> microcubes with different sizes. *Mater. Chem. Phys.* **2011**, *130*, 921–931. [[CrossRef](#)]
14. Jiang, H.; Zhao, L.; Gai, L.; Ma, L.; Maa, Y.; Lib, M. Hierarchical rh-In<sub>2</sub>O<sub>3</sub> crystals derived from InOOH counterparts and their sensitivity to ammonia gas. *Cryst. Eng. Comm.* **2013**, *15*, 7003–7009. [[CrossRef](#)]
15. Bal, A.K.; Singh, A.; Bedi, R.K. Characterization and room temperature sensing of ammonia and ethanol by thermally oxidized indium films. *Phys. B* **2010**, *405*, 3124–3128.
16. Guo, P.; Pan, H. Selectivity of Ti-doped In<sub>2</sub>O<sub>3</sub> ceramics as an ammonia sensor. *Sens. Actuators B* **2006**, *114*, 762–767. [[CrossRef](#)]
17. Shen, X.; Li, L.; Wu, Z.; Lü, H.; Lü, J. Ultrasonic-Assisted Acid Leaching of Indium from Blast Furnace Sludge. *Metall. Mater. Trans. B* **2013**, *44*, 1324–1328. [[CrossRef](#)]
18. Hasegawa, H.; Rahman, I.M.M.; Umehara, Y.; Sawai, H.; Maki, T.; Furusho, Y.; Mizutani, S. Selective recovery of indium from the etching waste solution of the flat-panel display fabrication process. *Microchem. J.* **2013**, *110*, 133–139. [[CrossRef](#)]
19. Hsieh, S.-J.; Chen, C.-C.; Say, W.C. Process for recovery of indium from ITO scraps and metallurgic microstructures. *Mater. Sci. Eng. B* **2009**, *158*, 82–87. [[CrossRef](#)]
20. Li, Y.; Liu, Z.; Li, Q.; Liu, Z.; Zeng, L. Recovery of indium from used indium-tin oxide (ITO) targets. *Hydrometallurgy* **2011**, *105*, 207–212. [[CrossRef](#)]
21. Virolainen, S.; Ibane, D.; Paatero, E. Recovery of indium from indium tin oxide by solvent extraction. *Hydrometallurgy* **2011**, *107*, 56–61. [[CrossRef](#)]
22. Gupta, B.; Deep, A.; Malik, P. Liquid–liquid extraction and recovery of indium using Cyanex 923. *Anal. Chim. Acta* **2004**, *513*, 463–471. [[CrossRef](#)]
23. Liu, G. Synthesis, characterization of In<sub>2</sub>O<sub>3</sub> nanocrystals and their photoluminescence property. *Inter. J. Electrochem. Sci.* **2011**, *6*, 2162–2170.
24. Yuan, Z.; Zhang, J.; Liu, G. Synthesis of In<sub>2</sub>O<sub>3</sub> nanocrystals via hydro/solvothermal route and their photoluminescence properties. *Inter. J. Electrochem. Sci.* **2013**, *8*, 1794–1801.
25. Souza, E.C.C.; Rey, J.F.Q.; Muccillo, E.N.S. Synthesis and characterization of spherical and narrow size distribution indium oxide nanoparticles. *Appl. Sur. Sci.* **2009**, *255*, 3779–3783. [[CrossRef](#)]
26. Nizhnik, O.; Higuchi, K.; Maenaka, K. Self-calibrated humidity sensor in CMOS without post-processing. *Sensors* **2012**, *12*, 226–232. [[CrossRef](#)] [[PubMed](#)]
27. Konvalina, G.; Haick, H. Effect of humidity on nanoparticle-based chemiresistors: a comparison between synthetic and real-world samples. *Appl. Mater. Interfaces* **2012**, *4*, 317–325. [[CrossRef](#)] [[PubMed](#)]
28. Shehada, N.; Brönstrup, G.; Funke, K.; Christiansen, S.; Leja, M.; Haick, H. Ultrasensitive silicon nanowire for real-world gas sensing: noninvasive diagnosis of cancer from breath volatolome. *Nano Lett.* **2015**, *15*, 1288–1295. [[CrossRef](#)] [[PubMed](#)]
29. Wang, B.; Cancilla, J.C.; Torrecilla, J.S.; Haick, H. Artificial sensing intelligence with silicon nanowires for ultrasensitive detection in the gas phase. *Nano Lett.* **2014**, *14*, 933–938. [[CrossRef](#)] [[PubMed](#)]



© 2015 by the authors; licensee MDPI, Basel, Switzerland. This article is an open access article distributed under the terms and conditions of the Creative Commons by Attribution (CC-BY) license (<http://creativecommons.org/licenses/by/4.0/>).